

High brightness single mode source of correlated photon pairs using a photonic crystal fiber

J. Fulconis¹, O. Alibart¹, W. J. Wadsworth², P. St.J. Russell² and J. G. Rarity¹

¹Centre for Communications Research, Department of Electrical and Electronic Engineering, University of Bristol, Merchant Venturers Building, Woodland Road, Bristol, BS8 1UB, United Kingdom.

Jeremie.Fulconis@bristol.ac.uk

²Photonics & Photonic Materials Group, Department of Physics, University of Bath, Claverton Down, Bath, BA2 7AY, UK

Abstract: We demonstrate a picosecond source of correlated photon pairs using a micro-structured fibre with zero dispersion around 715 nm wavelength. The fibre is pumped in the normal dispersion regime at ~ 708 nm and phase matching is satisfied for widely spaced parametric wavelengths. Here we generate up to 10^7 photon pairs per second in the fibre at wavelengths of 587 nm and 897 nm, while on collecting this light in single-mode-fibre-coupled Silicon avalanche diode photon counting detectors, we detect $\sim 3.2 \times 10^5$ coincidences per second at pump power 0.5 mW.

©2005 Optical Society of America

OCIS codes: (060.4370) Nonlinear optics fibers ; (270.0270) Quantum Optics.

References and Links

1. J. G. Rarity, Quantum Communications and Beyond, Royal Society Philosophical Transactions, **361**, 1507-18 (2003).
2. S. Gasparoni, J-W. Pan, P. Walther, T. Rudolph, and A. Zeilinger, "Realization of a Photonic Controlled-NOT Gate Sufficient for Quantum Computation," Phys. Rev. Lett. **93**, 020504 (2004).
3. P. Walther, K. J. Resch, T. Rudolph, E. Schenck, H. Weinfurter, V. Vedral, M. Aspelmeyer & A. Zeilinger, "Experimental one-way quantum computing," Nature **434**, 169 (2005).
4. N. Gisin, G. Ribordy, W. Tittel and H. Zbinden, "Quantum Cryptography," Rev. Mod. Phys. **74**, 145 (2002).
5. H. Weinfurter, "Quantum Communications, "Quantum communication with entangled photons," Adv. At. Mol. Opt. Phys. **42**, 489 (2000).
6. P. G. Kwiat, K. Mattle, H. Weinfurter, A. Zeilinger, A. V. Sergienko, and Y.H. Shih, "New High Intensity Source of Entangled Photon Pairs," Phys. Rev. Lett **75**, 4337 (1995).
7. C. Kurtsiefer, M. Oberparleiter, and H. Weinfurter, "High Efficiency entangled pair collection in type II parametric fluorescence," Phys. Rev. Lett. **85**, 290-293 (2000).
8. R. Andrews, E. R. Pike, and S. Sarkar, "Optimal coupling of entangled photons into single-mode optical fibers," Opt. Express **12**, 3264-3269 (2004), <http://www.opticsexpress.org/abstract.cfm?URI=OPEX-12-14-3264>
9. G. Bonfrate, V. Pruneiri, P. Kazanski, P. R. Tapster and J. G. Rarity, "Parametric fluorescence in periodically poled silica fibres," Appl. Phys. Lett. **75**, 2356 (1999).
10. S. Tanzilli, H. de Riedmatten, W. Tittel, H. Zbinden, P. Baldi, M. de Micheli, D. B. Ostrowski, N. Gisin, "Highly efficient photon-pair source using periodically poled lithium niobate waveguide," Electron. Lett. **37**, 26-28 (2001).
11. A. B. U'Ren, C. Silberhorn, K. Banaszek, and I. A. Walmsley, "Efficient Conditional Preparation of High-Fidelity Single Photon States for Fiber-Optic Quantum Networks," Phys. Rev. Lett. **93**, 601 (2004)
12. G. P. Agrawal, *Nonlinear fiber optics* (Academic, 1995).
13. L. J. Wang, C. K. Hong, and S. R. Friberg, "Generation of correlated photons via four-wave mixing in optical fibres," J. Opt. B: Quantum and Semiclass. Opt. **3**, 346-352 (2001).
14. M. Fiorentino, P. L. Voss, J. E. Sharping, P. Kumar, "All-fibre photon pair source for quantum communications," IEEE Photonics Technol Lett. **14**, 983-5 (2002).
15. X. Li, J. Chen, P. Voss, J. E. Sharping, and P. Kumar, "All-fiber photon-pair source for quantum communications: Improved generation of correlated photons," Opt. Express **12**, 3737-3745 (2004). <http://www.opticsexpress.org/abstract.cfm?URI=OPEX-12-16-3737>
16. J. E. Sharping, J. Chen, X. Li, P. Kumar, "Quantum Correlated twin photons from microstructured fibre," Opt. Express **12**, 3086-3094 (2004). <http://www.opticsexpress.org/abstract.cfm?URI=OPEX-12-14-3086>
17. X. Li, P. L. Voss, & P. Kumar, "Optical-fiber source of polarization-entangled photon pairs in the 1550 nm telecom band," arXiv:quant-ph/0402191 (Feb 2004).

18. H. Takesue and K. Inoue, "Generation of polarization-entangled photon pairs and violation of Bell's inequality using spontaneous four-wave mixing in a fiber loop," *Phys. Rev. A* **70**, 031802 (R) (2004).
19. W. J. Wadsworth, N. Joly, J. C. Knight, T. A. Birks, F. Biancalana, P. St. J. Russell, "Supercontinuum and four-wave mixing with Q-switched pulses in endlessly single-mode photonic crystal fibres," *Opt. Express* **12**, 299-309 (2004). <http://www.opticsexpress.org/abstract.cfm?URI=OPEX-12-2-299>
20. W. J. Wadsworth, P. St. J. Russell, J. G. Rarity, J. Duligall, J. R. Fulconis: "Single-mode source of correlated photon pairs from photonic crystal fibre," International Quantum Electronics Conference, CLEO/IQEC San Francisco, paper IPDA7 (2004)
21. J. G. Rarity, J. Fulconis, J. Duligall, W. J. Wadsworth, and P. S. J. Russell, "Photonic crystal fiber source of correlated photon pairs," *Opt. Express* **13**, 534-544 (2005). <http://www.opticsexpress.org/abstract.cfm?URI=OPEX-13-2-534>
22. Dougherty D J, Kärtner F X, Haus H A and Ippen E P 1995 Measurement of the Raman gain spectrum of optical fibers *Opt. Lett.* **20** 31-3
23. J G Rarity, "Interference of single photons from separate sources," in FUNDAMENTAL PROBLEMS IN QUANTUM THEORY D M Greenberger and A Zeilinger eds, Annals of the New York Academy of Sciences, 1995 p.624.
24. J.C. Knight, J. Arriaga, T.A. Birks, A. Ortigosa-Blanch, W.J. Wadsworth, P.St.J. Russell, "Anomalous dispersion in photonic crystal fiber," *IEEE Photonics Technol Lett.* **12** (7), 807-809 (2000).
25. J G Rarity, K D Ridley and P R Tapster, "An absolute measurement of detector quantum efficiency using parametric down-conversion," *Appl. Opt.* **26**, 4616-4619 (1987).
26. Perkin Elmer SPCM data sheet: <http://optoelectronics.perkinelmer.com/content/Datasheets/SPCM-AQR.pdf>
27. During the preparation of the manuscript other groups have obtained comparable brightness in similar fibres: see J. Fan, A. Migdall and L-J Wang, quant-ph 0505211
28. S.G. Leon-Saval, T.A. Birks, N.Y. Joly, A.K. George, W.J. Wadsworth, G. Kakarantzas and P.St.J. Russell, "Splice-free interfacing of photonic crystal fibres," *Opt. Lett.* **30** (13), 1629-1631, (2005)

1. Introduction

High brightness sources of correlated and entangled photon pairs are required for various multiphoton and linear optical logic applications [1-3]. They also find useful application to quantum cryptography [4] and quantum communications [5]. The preferred sources for such experiments until recently have been three wave mixing in $\chi^{(2)}$ non-linear birefringent crystals [6-8]. These sources are inherently wide band, low brightness (per nanometer, per single mode) sources. More recently periodically poled fibres [8] and periodically poled waveguides have been shown to be useful pair photon sources [9, 10]. In poled fibres the low non-linearity limits the brightness while in planar waveguides the non-circular mode limits the coupling efficiency into single mode optical fibres.

It is well known that parametric gain can arise from the $\chi^{(3)}$ non-linearity in optical fibres [12,13] and phase matching can be achieved by using the modulation instability when pumping fibres in their anomalous dispersion regime. Various pair photon generation experiments have been performed in this regime [14-18]. The photon pairs are generated close to the pump wavelength and are always accompanied by a significant Raman background and careful filtering is required.

We have recently shown that phase matching can be obtained for widely spaced wavelengths by pumping photonic crystal fibre (PCF) close to the zero dispersion wavelength in the *normal* dispersion regime [19]. This allowed us to demonstrate a CW source of photon pairs at widely spaced wavelengths of 834 nm signal and 1404 nm idler by pumping at 1047nm wavelength [20, 21]. However the idler signal lies on the shoulder of the fifth order Raman peak which is still a significant source of background light. Here we choose fibre with the zero dispersion point in the near infra-red (715nm) and pump with a *picosecond pulsed* laser, blue-detuned a few nanometers into the normal dispersion regime. This generates photon pairs visible to efficient silicon-based photon counting detectors. The number of created photon pairs is proportional to the square of the peak intensity while the spontaneous Raman scattering grows roughly linearly. Hence the use of a picosecond laser in our experiment allows us to improve the brightness while reducing Raman background noise to negligible levels. At the power used we remain in the spontaneous Raman scattering region and see no stimulated Raman scattering [19,22].

We are seeking to develop a source which may be applicable for future quantum interference experiments involving three or more photons created as two or more pairs. Interference effects between separate pair-photons can be studied by overlapping photons with a time uncertainty shorter than their inverse bandwidth or coherence length [23]. This restricts us to sources pumped by ultra-short laser pulses where the bandwidth is of order nanometers and also requires a high efficiency of collection. We show in the following that our source is naturally narrow band (compared to other guided configurations) and is efficiently coupled into single mode optical fibers, thus being ideal for quantum interference experiments.

2. Theory

Here the main nonlinear process that has to be taken into account is four-wave mixing (FWM) where phase matching and conservation of energy give the Eqs. (1) and (2) [12]:

$$k_i + k_s - 2k_p + 2\gamma P_p = 0 \quad (1)$$

and

$$\omega_i + \omega_s = 2\omega_p \quad (2)$$

where $k_{i,s,p}$ are the wave-vectors (propagation constants) of the idler, signal and pump photons and $\omega_{i,s,p}$ their respective frequencies; P_p is the peak pump power and γ is the nonlinear coefficient of the fiber,

$$\gamma = \frac{2\pi n_2}{\lambda A_{eff}} \quad (3)$$

where $n_2 = 2 \times 10^{-20} \text{ m}^2/\text{W}$ is the nonlinear refractive index of silica, A_{eff} is the effective area of the fiber mode and λ is the pump wavelength. These phase-matching conditions will yield the wavelengths for peak gain in a given fiber, which will depend on the chromatic dispersion of the fiber.

Figure 1 shows the microstructured fiber used in our experiment. The fiber has a core diameter of $2 \mu\text{m}$ and a zero dispersion wavelength λ_0 defined at 715 nm . Figure 2 shows the phase matching diagram plotting signal and idler wavelength against the pump. This is calculated from Eqs. (1) and (2) using the dispersion curve for a simple strand of silica in air as a close approximation [24] to the fiber used in this experiment. A strand diameter of $2 \mu\text{m}$ was used which gives a zero dispersion wavelength at 715 nm as measured in the fibre.

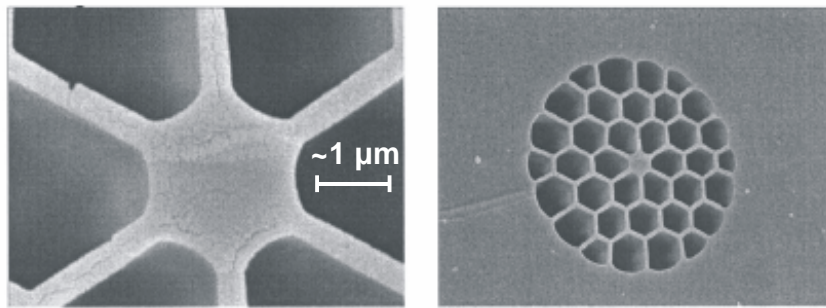


Fig. 1. Electron microscope image of the PCF used with core diameter $d \approx 2 \mu\text{m}$, $\lambda_0 = 715 \text{ nm}$

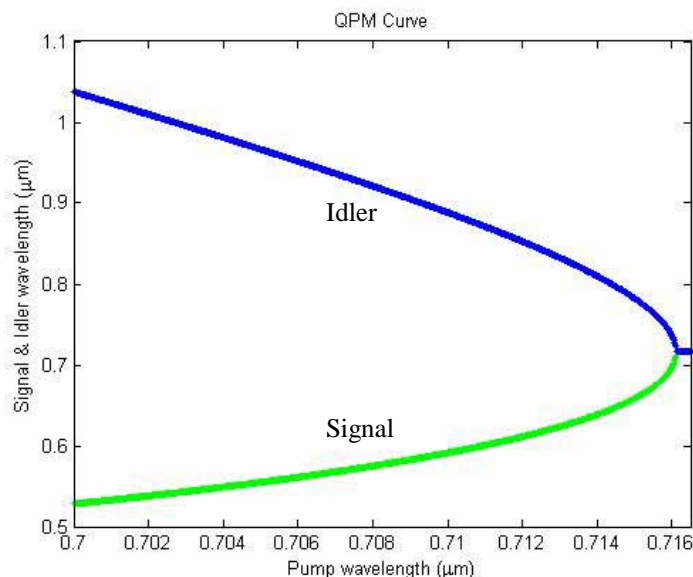


Fig. 2. Nonlinear phase-matching diagram for the process $2\omega_p \rightarrow \omega_s + \omega_i$. The curve does not change significantly in the range $P_p = 0-3$ W. Beyond the 716 nm “degeneracy” point we move into the modulation instability region where photon pairs can be created close to the pump wavelength (see [14-19]).

Since the number of created photon pairs is proportional to the square of the peak intensity while the Raman scattering grows roughly linearly, the use of a picosecond laser in our experiment allows us to improve the brightness but also to reduce the Raman source of background noise to negligible levels. For a given average power from the pump laser, the pair photon signal will scale as the inverse of the mark to space ratio of the pulses, whereas the Raman signal will be unchanged.

In our experiments we pump in the normal dispersion regime, where the sidebands generated are widely spaced at equal frequency intervals from the pump. The natural linewidth determined from the phase matching relations (when pumped by a monochromatic source) is below 0.2 nm. Hence we expect the bandwidth of parametric light generated by a picosecond pumped source to be mainly determined by the slope of phase matching curves multiplied by the pump bandwidth. Here we use a pulse full-width-half-maximum (FWHM) bandwidth of 0.3 nm (corresponding to a ~ 4 ps pulse) centered at 708.4 nm, which corresponds to a calculated FWHM bandwidth of 3.2 nm at 587 nm for the signal and 4.5 nm at 897 nm for the idler.

3. Experiment

In order to estimate the brightness of our source we used the coincidence setup depicted in Fig. 3 where a mode-locked picosecond Ti:Sapphire pump laser (Spectra Physics - Tsunami) set at 708.4 nm, emitting 4 ps pulses with a repetition rate of 80 Mhz is sent, through an optical isolator, onto a prism P to remove in-band light from the pump laser spontaneous emission. A pin hole is then used to improve the pump mode and eventually several attenuators bring the power down so that up to 540 μ W average power is launched into the fiber. Since the PCF is birefringent and supports two modes, a half wave-plate (HWP) is used to align the pump polarization along one axis thus preventing polarization scrambling and creating pairs with the same polarization as the pump beam. Compared to bulk crystal where the nonlinear interaction occurs actually at the pump beam focus, here the interaction will extend over the full length of the fiber and is thus more efficient. We then used for our

experiment 2 m of PCF allowing us to expect a high conversion efficiency. The output of the fiber is collimated using an aspheric lens, followed by a removable mirror M, allowing us to monitor the photon pair spectra in a monochromator or to launch them into a coincidence test bench. In this latter part of the setup, a dichroic mirror centered at 700 nm is used to spread the incoming beam into two arms, one corresponding to the *signal* channel and the other to the *idler*, where band-pass filters F1 and F2 centered at 570 nm and 880 nm respectively (width ~ 40 nm, $T > 80\%$) are used to remove in-line pump and background light. Each photon of the pair is then launched into single mode fibers that are connected to two Silicon avalanche photodiodes (APD). The detected photons are counted in a dual-channel counter and the coincidences between the two APDs are analyzed using a time interval analysis system (TIA).

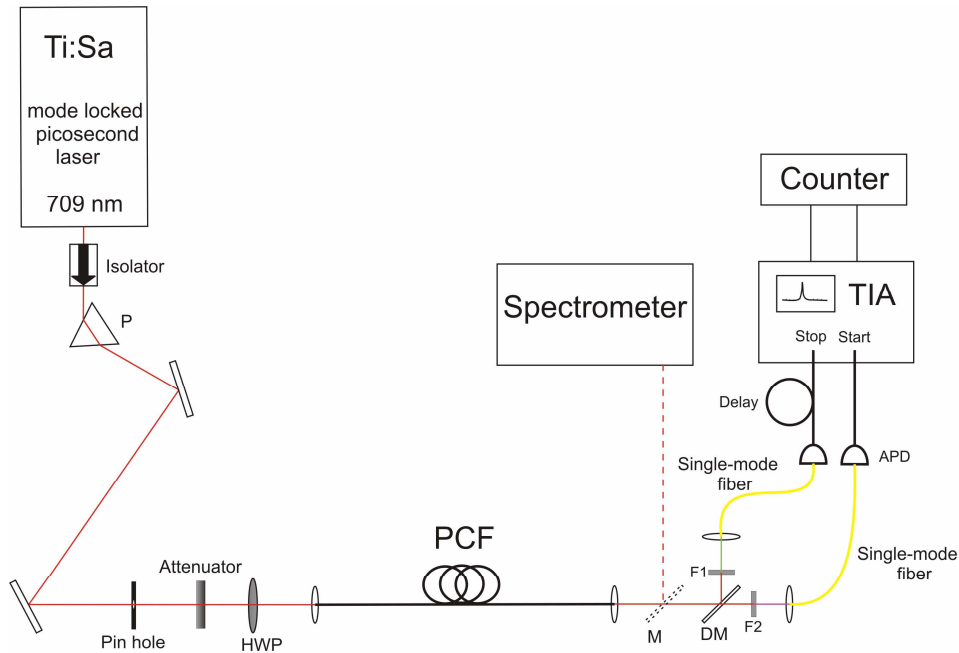


Fig. 3. Optical layout. Laser, 708 nm Ti:Sa laser; P, prism; HWP, halfwave plate; PCF, 2 m of photonic crystal fiber; M, protected silver mirror ($R > 95\%$); DM, dichroic mirror (centered @ 700 nm, $T > 85\%$, $R > 90\%$); F1, 570 nm band-pass filter, bandwidth 40 nm, $T = 80\%$; F2, 880 nm band-pass filter, bandwidth 40 nm, $T = 80\%$; APD, Silicon single photon detector.

4. Results

Pumping with 708.4 nm light and aligning the polarisation on one of the axes of the fiber, we see the narrowband pair-photon spectra illustrated in Fig. 4 and Fig. 5. The short wavelength sits at 587 nm and the corresponding idler at 897 nm. Note that these wavelengths are easily tunable using fiber parameters or pump wavelength thus allowing us to set the signal and idler photon far from the degeneracy point ($\lambda_0 = 715$ nm) where the noise from Raman background is negligible. The pair emission is narrow band and we measure 2.7 nm and 5.5 nm FWHM bandwidths for the signal and idler respectively. These correspond well with the simple theory presented in section 2. The spectra were taken at a pump power of 700 μ W and flat background comes entirely from the electronic bias errors in the CCD amplification and analogue to digital converter (ADC) circuits. In the IR signal we see a very slight increase in background towards shorter wavelengths which we ascribe mainly to residual Raman scattering. The micro-structure makes the fiber slightly birefringent. As a consequence, when we do not launch into the correct fibre polarisation axis, we see two peaks corresponding to

different phase matching conditions for the different fibre axes. The absence of the second peak here implies our source is strongly polarised.

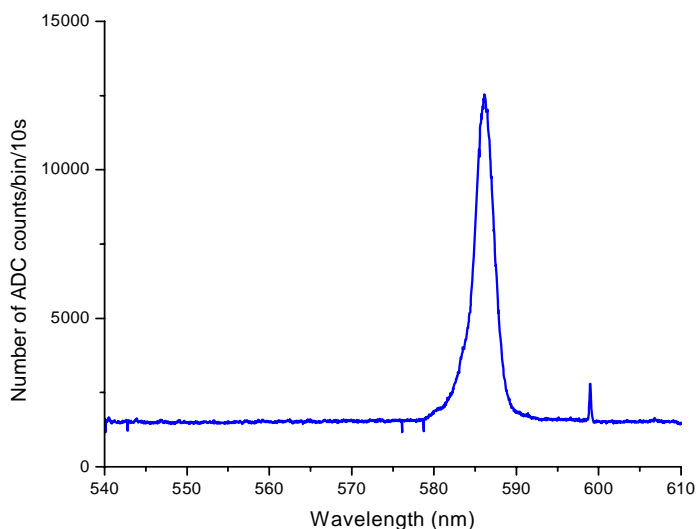


Fig. 4. Fluorescence spectrum of the signal photons. The measurement was integrated over 10 seconds. The number of ADC counts is proportional to the number of photons detected by the cooled camera in wavelength-bins of width 36 pm. The photon spectrum is centered at 587 nm and features a FWHM bandwidth of 2.7 nm. The small peak at 598 nm is attributed to unwanted background light or a detector fault. It is visible when the laser is blocked.

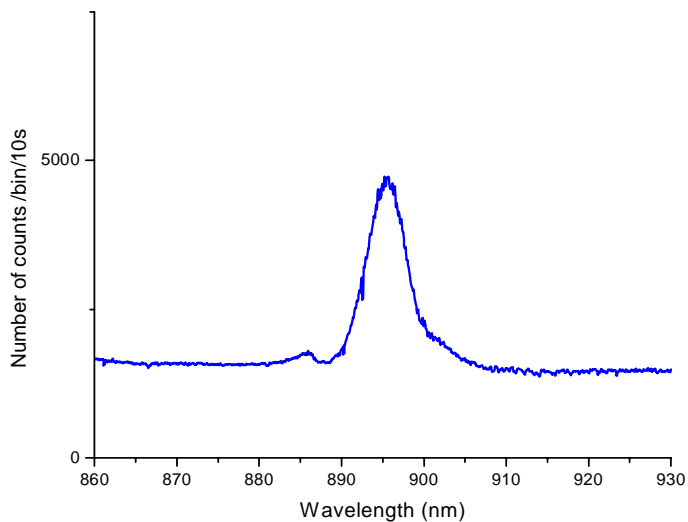


Fig. 5. Fluorescence spectrum of the idler photons. The measurement was integrated over 10 seconds. The photon spectrum is centered at 897 nm and features a FWHM bandwidth 5.5 nm. Here the wavelength-bin width is 36 pm.

Looking now at the coincidence test bench in order to determine the brightness of our source, we measured the number of single counts in both signal and idler channels, while we recorded the number of coincidences. This experimental protocol amounts to recording the percentage of detections in the “start channel” which have been stopped by detection in the “stop channel” in the following time interval and effectively provides a direct estimate of the “lumped” efficiency of the stop channel.

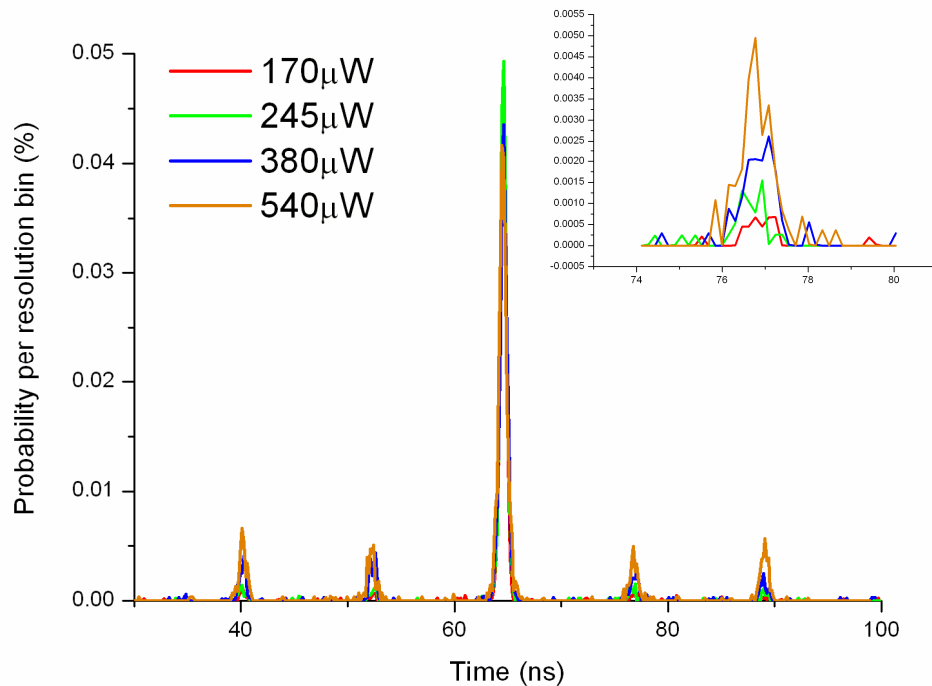


Fig. 6. Time interval histogram showing the coincident photon detection peak and also a zoom on one of the accidental coincidence peak for different pump powers. Here the time between two peaks reflects the pump laser repetition rate. However the width of the peaks is limited by the response time of the detectors which is typically hundreds of picoseconds (rather than the actual duration of the pump pulses). The instrument displays the probability that a start pulse is stopped within a given time bin. Here the time-bin width is 156 ps. To step through the pump powers press Ctrl + click on the graph.

The central peak corresponds to signal and idler photons belonging to the same pulse, whereas the small satellite peaks stand for uncorrelated events i.e. signal and idler coming from subsequent pulses (whether they are actual pairs of photons or Raman photon). It is interesting to note the satellite peaks grow with pump power, whereas the central peak remains constant. The central peak reflects the lumped collection efficiency which is relatively constant with increasing pump power (confirming correlated photon pair creation), while the satellite ones are linked to the probability of having a photon from a different pair or a Raman background photon in a neighbouring pulse. In the absence of background the satellite peaks would be indicative of the rate of generation of pairs of pairs, or 4-photon events. It is these events that could be useful for multi-photon interference experiments and quantum information applications. However, we also have to take into account both the Raman background and the multi-photon pair rate in the central peak as they increase the photon count probability. Thus we will introduce C_{raw} as the raw coincidence rate in the central peak and we will calculate the added accidental coincidence rate thanks to the satellites peaks C_b .

We can use the singles counting rates and the coincidence rates to estimate the actual rate of pairs created inside the PCF, using the following Eqs. [25]:

$$\begin{aligned} N_s &= \eta_s \eta_{opt} r + B_s \\ N_i &= \eta_i \eta'_{opt} r + B_i \\ C_{raw} &= \eta_s \eta_i \eta_{opt} \eta'_{opt} r + C_b \end{aligned} \quad (4)$$

where N_s , N_i are respectively the counting rates in the signal and idler APDs, while B_s , B_i are background rates including Raman photons and multi-photon pairs. η_s and η_i are the APD quantum efficiencies at 587 nm and 897 nm, the net optical transmission and launch efficiencies into single mode fibre of each arm are η_{opt} and η'_{opt} .

On one hand, if we neglect the background (Raman and multi-photon pairs), we could directly estimate the measured lumped efficiencies η_M^{lump} of each arm and the pair photon production rate r

$$\begin{aligned} \eta_{sM}^{lump} &= \frac{C_{raw} - C_b}{N_i} \\ \eta_{iM}^{lump} &= \frac{C_{raw} - C_b}{N_s} \\ r &= \frac{C_{raw} - C_b}{\eta_{iM}^{lump} \eta_{sM}^{lump}} \end{aligned} \quad (5)$$

On the other hand, we can also estimate these lumped efficiencies directly from the detector data sheet [26] and from classical loss measurement on our collection setup. We found $\eta_s \sim 0.6$ and $\eta_i \sim 0.33$, while the launch efficiencies into single mode fiber of each arm are estimated to be 60-65%. When combined with the measured transmission of lenses and filters (presented in Fig. 3 caption) we estimate $\eta_{opt} \sim 0.35-0.38$, $\eta'_{opt} \sim 0.33-0.36$ (including fiber coupling, filters, dichroic mirror and lenses losses for signal and idler channels respectively). This then gives us an estimate of $\eta_{sP}^{lump} \sim 0.211-0.229$ and $\eta_{iP}^{lump} \sim 0.11-0.119$ where the subscript P denotes “predicted”. It becomes clear that any difference between the “measured” and “predicted” lumped efficiencies would arise from the background we neglected earlier in Eq. (5). We can then roughly estimate the background contributions by combining Eqs. (4) and (5) to give

$$\begin{aligned} \frac{\eta_{sM}^{lump}}{\eta_{sP}^{lump}} &= \left(1 - \frac{B_i}{N_i} \right) \\ \frac{\eta_{iM}^{lump}}{\eta_{iP}^{lump}} &= \left(1 - \frac{B_s}{N_s} \right) \end{aligned} \quad (6)$$

We then took several measurements for a range of different pump powers so that the ratio of Raman background to signal would change thus changing the ratios B/N in Eqs. (6) and compared the measured and predicted efficiencies. The results are shown in the following Table 1.

Table 1. Summary of results for different pump powers

Pump Power P	170 μ W	245 μ W	380 μ W	540 μ W
N_s	$3.4 \times 10^5 \text{ s}^{-1}$	$6.8 \times 10^5 \text{ s}^{-1}$	$1.57 \times 10^6 \text{ s}^{-1}$	$2.89 \times 10^6 \text{ s}^{-1}$
N_i	$1.9 \times 10^5 \text{ s}^{-1}$	$3.6 \times 10^5 \text{ s}^{-1}$	$8.2 \times 10^5 \text{ s}^{-1}$	$1.52 \times 10^6 \text{ s}^{-1}$
C_{raw}	$3.9 \times 10^4 \text{ s}^{-1}$	$8.0 \times 10^4 \text{ s}^{-1}$	$1.8 \times 10^5 \text{ s}^{-1}$	$3.6 \times 10^5 \text{ s}^{-1}$
C_b	$0.1 \times 10^4 \text{ s}^{-1}$	$0.2 \times 10^4 \text{ s}^{-1}$	$0.1 \times 10^5 \text{ s}^{-1}$	$0.4 \times 10^5 \text{ s}^{-1}$
$C = C_{raw} - C_b$	$3.8 \times 10^4 \text{ s}^{-1}$	$7.8 \times 10^4 \text{ s}^{-1}$	$1.7 \times 10^5 \text{ s}^{-1}$	$3.2 \times 10^5 \text{ s}^{-1}$
Measured signal efficiency η_{sM}^{lump} Eq. (5)	20.0 %	21.7 %	20.7 %	21.1%
Predicted signal efficiency η_{sP}^{lump}	21.1-22.9%			
B_i/N_i from Eq. (6)	0.052-0.126	0-0.052	0.019-0.096	0-0.08
Measured idler efficiency η_{iM}^{lump} Eq. (5)	11.2 %	11.5 %	10.8 %	11.1 %
Predicted idler efficiency η_{iP}^{lump}	11.0-11.9%			
B_s/N_s from Eq. (6)	0-0.059	0-0.034	0.018-0.092	0-0.067
Photon pair production rate in the fibre r (Eq. (5))	$1.7 \times 10^6 \text{ s}^{-1}$	$3.1 \times 10^6 \text{ s}^{-1}$	$7.6 \times 10^6 \text{ s}^{-1}$	$1.4 \times 10^7 \text{ s}^{-1}$
Average number of pairs per pulse	0.021	0.039	0.095	0.18

From Table 1, we see that we have measured up to 3.2×10^5 net coincidences per second. We also see that the lower estimated idler efficiency is below the measured value suggesting that the fibre launch efficiency is higher than our lower estimate at $\sim 62\%$. Therefore if we look at the higher estimated efficiency, it confirms that the background in the signal count rate (green) is very low ($< 5\%$ of the total rate), as expected as there is no Raman signal in the green. In the infra-red we estimate a background that varies between 3% and 10% of the count rate whatever is the pump power. This is counter to our expectation of a reduction of background at higher pump powers and may simply be due to our rather crude analysis. Indeed we have taken no account of dead-time corrections in the detectors and time interval analyser and only a simple account of multi-photon effects. We are presently making an independent measure of the background to confirm these results. At this stage we can say that background in the IR is smaller than 10% of the signal for all powers measured.

5. Discussion

In Fig. 7 we plot the coincidence rate as a function of pump power. We clearly see a purely quadratic behaviour. Thus we cannot present our rates in terms of coincidences per milliwatt per nanometre. However we have seen 320,000 net coincidences per second with pump powers of 0.54 mW (or $\sim 1.2 \times 10^6 / \text{sec/mW}^2$) with natural bandwidths of signal 2.7 nm and idler 5.5 nm. This is this brightest source of pair photons and heralded single photons that we know of [27]. Our source is limited in brightness by two principle factors. The first is saturation of the detectors and coincidence measuring equipment, which is causing significant distortion at the highest pump powers. The second is the optical losses and detector efficiencies.

A preliminary experiment using a multimode fiber in the signal channel showed efficiency in the signal arm going up to 33% due to high coupling efficiency (>95%) in multimode fiber. This result highlights the limited launch efficiency into single-mode fibers, which we estimate to be about 62%. Although this value is already better than any nonlinear waveguide [10] solution to our knowledge, we expect this efficiency to be improved to >80% using a pigtailed fiber [28] which will compare favourably with the best results from bulk nonlinear crystal [7].

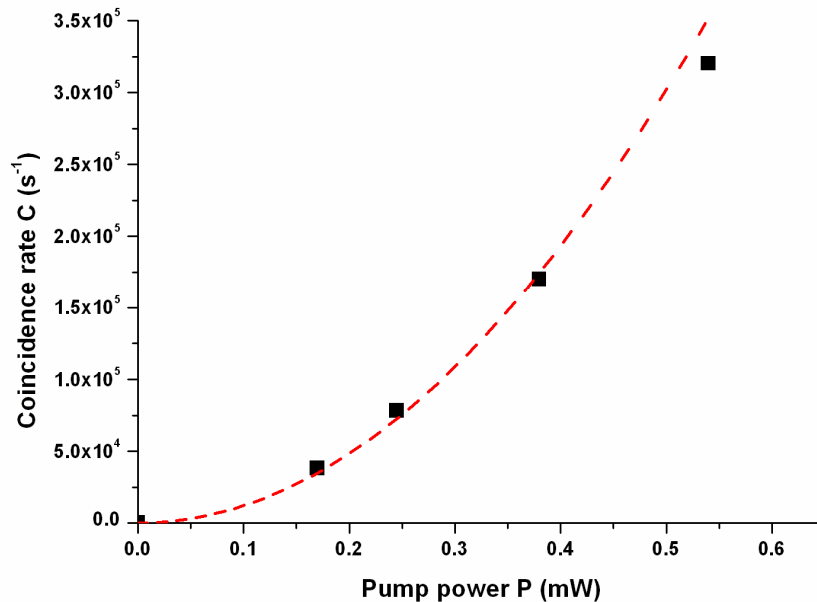


Fig. 7. Net coincidence rate as function of the pump power. The fit is purely quadratic (no linear term) $C=AP^2$ with constant $A=1.21 \times 10^6$ /sec/mW². Discrepancies at high powers are due to saturation effects in both the detectors and coincidence measuring apparatus.

It is also worth discussing the Raman background. The Raman scattering produces about 13 THz frequency shift per order. At the idler wavelength we are between the 6th and 7th order. This is the main reason for our low Raman background. At the powers we are using we will only ever see spontaneous Raman scattering at this order and in this length of fibre [19]. This means the Raman grows linearly with increasing pump power. In Fig. 6 we would expect the satellite peaks to decrease in significance as we increase pump power as the ratio B_i/N_i decreases, if they were dominated by spontaneous Raman scattering. The satellite peaks in figure 6 actually increase clearly showing that the background coincidence rate at high counting rates is dominated by random overlap of more than one pair of photons. We thus do not to present our data in terms of the ratio of coincidence rate to background coincidence rate. We work here only with the measured efficiencies of 20.7±0.3% in the signal (green) and 11.3±0.2% in the idler (IR) which are more significant. Since the background coincidence rate is linked to the multi-photon pair probability, it is indicative of the four photon coincidence rate we will get in future experiments and is a variable we want to maximise.

For these multi-photon quantum information experiments we require a narrower bandwidth so that the coherence length is equivalent to the pulse length [23]. A quantum interference experiment involving four-fold coincidence between photons coming from two separated sources would require a filter of order 0.2 nm bandwidth in the Green (0.4nm in the IR). Such filters will transmit only 40% of in-band light thus halving our effective efficiencies and collect only $\sim 1/15$ of the available spectrum. However counting rates would be significantly reduced thus allowing an increase in pump power. Using our source with a pump power of 2 mW, the expected rate of photon pairs detected within this bandwidth is $>8 \cdot 10^4$ /s, which means a rate of four photon events $>80 \text{ s}^{-1}$, two orders of magnitude higher than any previous experiment.

6. Conclusion

We have reported the measurement of picosecond-pulsed photon pairs generated by four-wave mixing in a single-mode optical fiber, pumped in the normal dispersion regime. The source is polarized, bright, narrowband, single-mode and tunable by varying laser wavelength or fiber parameters. The wide separation of the generated pair wavelengths means that most of the background can be avoided. All these advantages make this new source of photon pairs more appropriated compared to conventional ones for quantum information processing applications.

Acknowledgments

WJW is a Royal Society University Research Fellow. The authors would like to thank D. (ripper) Wardle for early input. The work is partly funded by UK EPSRC QIP IRC and EU IST-2001-38864 RAMBOQ.